

研究成果の刊行に関する一覧表

書籍

著者氏名	論文タイトル名	書籍全体の 編集者名	書 籍 名	出版社名	出版地	出版年	ページ

雑誌

発表者氏名	論文タイトル名	発表誌名	巻号	ページ	出版年
<u>Izumi R, Niihori T, Aoki Y, Suzuki N, Kato M, Warita H, Takahashi T, Tateyama M, Nagashima T, Funayama R, Abe K, Nakayama K, Aoki M, Matsubara Y.</u>	Exome sequencing identifies a novel TTN mutation in a family with hereditary myopathy with early respiratory failure.	J Hum Genet	58(5)	259-66	2013
<u>Aoki Y, Niihori T, Banjo T, Okamoto N, Mizuno S, Kurosawa K, Ogata T, Takada F, Yano M, Ando T, Hoshika T, Barnett C, Ohashi H, Kawame H, Hasegawa T, Okutani T, Nagashima T, Hasegawa S, Funayama R, Nagashima T, Nakayama K, Inoue SI, Watanabe Y, Ogura T, Matsubara Y.</u>	Gain-of-function mutations in RIT1 cause Noonan syndrome, a RAS/MAPK pathway syndrome.	Am J Hum Genet	93	173-80	2013

Witt H, Beer S, Rosendahl J, Chen JM, Chandak GR, Masamune A, Bence M, Szmola R, Oracz G, Macek M Jr, Bhatia E, Steigenberger S, Lasher D, Bühler F, Delaporte C, Tebbing J, Ludwig M, Pilsak C, Saum K, Bugert P, Masson E, Paliwal S, Bhaskar S, Sobczynska-Tomaszewska A, Bak D, Balascak I, Choudhuri G, Nageshwar Reddy D, Rao GV, Thomas V, Kume K, Nakano E, Kakuta Y, <u>Shimosegawa T</u> et al.(67人)	Variants in CPA1 are strongly associated with early onset chronic pancreatitis.	Nat Genet	45	1216-20.	2013
Sekiguchi K, Maeda T, Suenobu S, Kunisaki N, Shimizu M, Kiyota K, Handa YS, Akiyoshi K, Korematsu S, <u>Aoki Y</u> , <u>Matsubara Y</u> , Izumi T.	A transient myelodysplastic/myeloproliferative neoplasm in a patient with cardio-facio-cutaneous syndrome and a germline BRAF mutation.	Am J Med Genet A	161(10)	2600-3	2013
Takahashi T, <u>Aoki M</u> , et al.,	Clinical features and a mutation with late onset of limb girdle muscular dystrophy 2B.	J Neurol Neurosurg Psychiatry	84:	433-40	2013
Yamamoto A, Nakamura K, Matsumoto S, Iwai M, Shigematsu Y, Tajima G, Tsumura M, Okada S, Mitsubuchi H, <u>Endo F</u>	VLCAD deficiency in a patient who recovered from ventricular fibrillation, but died suddenly of a respiratory syncytial virus infection.	Pediatr Int	55(6)	775-778	2013

Kido J, Nakamura K, Matsumoto S, Mitsubuchi H, Ohura T, Shigematsu Y, Yorifuji T, Kasahara M, Horikawa R, Endo F	Current status of hepatic glycogen storage disease in Japan: clinical manifestations, treatments and long-term outcomes.	J Hum Genet	58(5)	285-292	2013
Fujisawa D, Nakamura K, Mitsubuchi H, Ohura T, Shigematsu Y, Yorifuji T, Kasahara M, Horikawa R, Endo F	Clinical features and management of organic acidemias in Japan.	J Hum Genet	58	769-74	2013
Fukami M, Tsuchiya T, Vollbach H, Ogata T, et al.	Genomic basis of aromatase excess syndrome: recombination- and replication-mediated rearrangements leading to <i>CYP19A1</i> overexpression.	J Clin Endocrinol Metab	98 (12)	E2013–2021	2013
Igarashi M, Dung VC, Suzuki E, Ogata T, Fukami M, et al.	Cryptic genomic rearrangements in three patients with 46,XY disorders of sex development.	PLoS One	8 (7)	e68194	2013
Fukami M, Iso M, Sato N, Ogata T, et al.	Submicroscopic deletion involving the fibroblast growth factor receptor 1 gene in a patient with combined pituitary hormone deficiency.	Endocr J	60 (8)	1013–1020	2013

Nakagawa K, Gonzalez-Roca E, Souto A, Kawai T, Umebayashi H, Campistol JM, Cañellas J, Takei S, Kobayashi N, Callejas-Rubio JL, Ortego-Centeno N, Ruiz-Ortiz E, Rius F, Anton J, Iglesias E, Jimenez-Treviño S, Vargas C, Fernandez-Martin J, Calvo I, Hernández-Rodríguez J, Mendez M, Dordal MT, Basagaña M, Bujan S, Yashiro M, Kubota T, Koike R, Akuta N, Shimoyama K, Iwata N, Saito MK, Ohara O, Kambe N, Yasumi T, Izawa K, Kawai T, Heike T, Yagüe J, Nishikomori R, Aróstegui JJ.	Somatic NLRP3 mosaicism in Muckle-Wells syndrome. A genetic mechanism shared by different phenotypes of cryopyrin-associated periodic syndromes.	Ann Rheum Dis	Dec 10	[Epub ahead of print]	2013
Wada T, Sakakibara Y, Nishimura R, Toma T, Ueno Y, Horita S, Tanaka T, Nishi M, Kato K, Yasumi T, Ohara O, Yachie A.	Down-regulation of CD5 expression on activated CD8(+) T cells in familial hemophagocytic lymphohistiocytosis with perforin gene mutations.	Hum Immunol	74:12	1579-1585	2013
Lee YW, Yang EA, Kang HJ, Yang X, Mitsuiki N, Ohara O, Miyawaki T, Kanegane H, Lee JH.	Novel mutation of IL2RG gene in a Korean boy with X-linked severe combined immunodeficiency.	J Invest Allergol Clin Immunol	23:1	65-67	2013
Kamae C, Nakagawa N, Sato H, Honma K, Mitsuiki N, Ohara O, Kanegane H, Pasic S, Pan-Hammarström Q, van Zelm MC, Morio T, Imai K, Nonoyama S.	Common variable immunodeficiency classification by quantifying T-cell receptor and immunoglobulin κ-deleting recombination excision circles.	J Allergy Clin Immunol	131:5	1437-1440	2013

Numata Y, Morimura T, Nakamura S, Hirano E, <u>Kure S</u> , Goto YI, Inoue K.	Depletion of molecular chaperones from the endoplasmic reticulum and fragmentation of the Golgi apparatus associated with pathogenesis in Pelizaeus-Merzbacher disease.	J Biol Chem	288	7451-66	2013
Horino S, Uchiyama T, So T, Nagashima H, Sun SL, Sato M, Asao A, Haji Y, Sasahara Y, Candotti F, Tsuchiya S, <u>Kure S</u> , Sugamura K, Ishii N.	Gene therapy model of X-linked severe combined immunodeficiency using a modified foamy virus vector.	PLoS One	8	e71594	2013
Watanabe Y, Sasahara Y, Ramesh N, Massaad MJ, Yeng Looi C, Kumaki S, <u>Kure S</u> , Geha RS, Tsuchiya S.	T-cell receptor ligation causes Wiskott-Aldrich syndrome protein degradation and F-actin assembly downregulation.	J Allergy Clin Immunol	132	648-655	2013
Masamune A, Nakano E, Kume K, Kakuta Y, Ariga H, <u>Shimosegawa T</u> .	Identification of novel missense CTRC variants in Japanese patients with chronic pancreatitis.	Gut	62	653-4	2013
Masamune A, Nakano E, Kume K, Takikawa T, Kakuta Y, <u>Shimosegawa T</u> .	PRSS1 c.623G>C (p.G208A) variant is associated with pancreatitis in Japan.	Gut	63	366	2014
Narumi Y, Min BJ, Shimizu K, Kazukawa I, Sameshima K, Nakamura K, Kosho T, Rhee Y, Chung YS, Kim OH, <u>Fukushima Y</u> , Park WY, Nishimura G.	Clinical consequences in truncating mutations in exon 34 of NOTCH2: report of six patients with Hajdu-Cheney syndrome and a patient with serpentine fibula polycystic kidney syndrome.	Am J Med Genet A	161A	518-526	2013
Purevsuren J, Kobayashi H, Hasegawa Y, Yamada K, Takahashi T, Takayanagi M, Fukao T, Fukuda S, <u>Yamaguchi S</u>	Intracellular in vitro probe acylcarnitine assay for identifying deficiencies of carnitine transporter and carnitine palmitoyltransferase-1	Anal Bioanal Chem	405(4)	1345-1351	2013

<u>Yamaguchi S</u> , Purevusren J, Kobayashi H, Hasegawa Y, Mushimoto Y, Yamada K, Takahashi T, Furui M, Taketani T, Fukuda S, Fukao T, Shigematsu Y	Expanded newborn mass screening with MS/MS and medium-chain acyl-CoA dehydrogenase (MCAD) deficiency in Japan	日本マススクリー ーニング学会誌	23(3)	270-276	2013
<u>Tomita H</u> , Ziegler ME, Kim HB, Evans SJ, Choudary PV, Li JZ, Meng F, Dai M, Myers RM, Neal CR, Speed TP, Barchas JD, Schatzberg AF, Watson SJ, Akil H, Jones EG, Bunney WE, Vawter MP.	G protein-linked signaling pathways in bipolar and major depressive disorders.	Front Genet	23(4): 21-12 97.		2013
Shi D, Takano Y, Nakazawa T, Mengkegale M, Yokokura S, Nishida K, <u>Fuse N</u> .	Molecular Genetic Analysis of Primary Open-angle Glaucoma, Normal Tension Glaucoma, and Developmental Glaucoma for the VAV2 and VAV3 Gene Variants in Japanese Subjects.	Biochem Biophys Res Commun	432	509-512	2013
Tsuda S, Yokoyama Y, Chiba N, Aizawa N, Shiga Y, Yasuda M, Yokokura S, Otomo T, <u>Fuse N</u> , Nakazawa T.	Effect of Topical Tafluprost on Optic Nerve Head Blood Flow in Patients With Myopic Disc Type.	J Glaucoma	22	398-403	2013
Hosogane M, <u>Funayama R</u> , Nishida Y, <u>Nagashima T</u> , <u>Nakayama K</u> .	Ras-Induced Changes in H3K27me3 Occur after Those in Transcriptional Activity.	PLoS Genet	9	e1003698	2013
Ninomiya M, Kondo Y, <u>Funayama R</u> , <u>Nagashima T</u> , Kogure T, Kakazu E, Kimura O, Ueno Y, <u>Nakayama K</u> , <u>Shimosegawa T</u> .	Distinct MicroRNAs Expression Profile in Primary Biliary Cirrhosis and Evaluation of miR 505-3p and miR197-3p as Novel Biomarkers.	PLoS One	8	e66086	2013

Sun SL, Horino S, Itoh-Nakadai A, Kawabe T, Asao A, Takahashi T, So T, <u>Funayama R</u> , Kondo M, Saitsu H, Matsumoto N, <u>Nakayama K</u> , Ishii N.	Y chromosome-linked B and NK cell deficiency in mice.	J Immunol	190	6209-20	2013
Ninomiya M, Kondo Y, <u>Niihori T</u> , Nagashima T, Kogure T, Kakazu E, Kimura O, <u>Aoki Y</u> , <u>Matsubara Y</u> , <u>Shimosegawa T</u> .	Sequential analysis of amino acid substitutions with hepatitis B virus in association with nucleoside/nucleotide analog treatment detected by deep sequencing.	Hepatol Res	May 24	[Epub ahead of print]	2013
Sakano D, Shiraki N, Kikawa K, Yamazoe T, Kataoka M, Umeda K, Araki K, Mao D, Matsumoto S, Nakagata N, Andersson O, Stainier D, <u>Endo F</u> , Kume K, Uesugi M, Kume S	VMAT2 identified as a regulator of late-stage β -cell differentiation.	Nat Chem Biol	10(2)	141-148	2014
Yamazaki T, Murayama K, Compton AG, Sugiana C, Harashima H, Amemiya S, Ajima M, Tsuruoka T, Fujinami A, Kawachi E, Kurashige Y, Matsushita K, Wakiguchi H, Mori M, Iwasa H, Okazaki Y, Thorburn DR, <u>Ohtake A</u>	Molecular diagnosis of mitochondrial respiratory chain disorders in Japan: Focusing on mitochondrial DNA depletion syndrome.	Pediatr Int	56 (2)	in press	2014
<u>Ohtake A</u> , Murayama, K, Mori M, Harashima H, Yamazaki T, Tamaru S, Yamashita I, Kishita Y, Nakachi Y, Kohda M, Tokuzawa Y, Mizuno Y, Moriyama Y, Kato H, Okazaki Y	Diagnosis and molecular basis of mitochondrial respiratory chain disorders: exome sequencing for disease gene identification.	Biochim Biophys Acta (General Subjects on Special Issue: Frontiers of Mitochondria.)		in press	2014

Tsuchiya T, Shibata M, Numabe H, <u>Ogata T</u> , et al.	Compound heterozygous deletions in pseudoautosomal region 1 in an infant with mild manifestations of Langer mesomelic dysplasia.	Am J Med Genet A	164A(2)	505-10	2014
Horino S, Sasahara Y, Sato M, Niizuma H, Kumaki S, Abukawa D, Sato A, Imaizumi M, Kanegane H, Kamachi Y, Sasaki S, Terui K, Ito E, Kobayashi I, Ariga T, Tsuchiya S, <u>Kure S</u> .	Selective expansion of donor-derived regulatory T cells after allogeneic bone marrow transplantation in a patient with IPEX syndrome.	Pediatr Transplant	18	E25-30	2014
Okae H, Matoba S, <u>Nagashima T</u> , Mizutani E, Inoue K, Ogonuki N, Chiba H, <u>Funayama R</u> , Tanaka S, Yaegashi N, <u>Nakayama K</u> , Sasaki H, Ogura A, <u>Arima T</u> .	RNA sequencing-based identification of aberrant imprinting in cloned mice.	Hum Mol Genet	23	992-1001	2014

(作成上の留意事項)

1. 「研究成果の刊行に関する一覧表」に記入した書籍又は雑誌は、その刊行物又は別刷り一部を添付すること。
2. 研究報告書（当該報告書に含まれる文献等を含む。以下本留意事項において同じ。）は、国立国会図書館及び厚生労働省図書館並びに国立保健医療科学院ホームページにおいて公表されるものであること。研究者等は当該報告書を提出した時点で、公表について承諾したものとすること。
3. 日本工業規格A列4番の用紙を用いること。各項目の記入量に応じて、適宜、欄を引き伸ばして差し支えない。

IV. 研究成果の刊行物・別刷

ORIGINAL ARTICLE

Exome sequencing identifies a novel *TTN* mutation in a family with hereditary myopathy with early respiratory failure

Rumiko Izumi^{1,2}, Tetsuya Niihori¹, Yoko Aoki¹, Naoki Suzuki², Masaaki Kato², Hitoshi Warita², Toshiaki Takahashi³, Maki Tateyama², Takeshi Nagashima⁴, Ryo Funayama⁴, Koji Abe⁵, Keiko Nakayama⁴, Masashi Aoki² and Yoichi Matsubara¹

Myofibrillar myopathy (MFM) is a group of chronic muscular disorders that show the focal dissolution of myofibrils and accumulation of degradation products. The major genetic basis of MFMs is unknown. In 1993, our group reported a Japanese family with dominantly inherited cytoplasmic body myopathy, which is now included in MFM, characterized by late-onset chronic progressive distal muscle weakness and early respiratory failure. In this study, we performed linkage analysis and exome sequencing on these patients and identified a novel c.90263G>T mutation in the *TTN* gene (NM_001256850). During the course of our study, another groups reported three mutations in *TTN* in patients with hereditary myopathy with early respiratory failure (HMERF, MIM #603689), which is characterized by overlapping pathologic findings with MFMs. Our patients were clinically compatible with HMERF. The mutation identified in this study and the three mutations in patients with HMERF were located on the A-band domain of titin, suggesting a strong relationship between mutations in the A-band domain of titin and HMERF. Mutation screening of *TTN* has been rarely carried out because of its huge size, consisting of 363 exons. It is possible that focused analysis of *TTN* may detect more mutations in patients with MFMs, especially in those with early respiratory failure.

Journal of Human Genetics (2013) 58, 259–266; doi:10.1038/jhg.2013.9; published online 28 February 2013

Keywords: A-band; cytoplasmic body; Fn3 domain; hereditary myopathy with early respiratory failure; HMERF; myofibrillar myopathy; titin; *TTN*

INTRODUCTION

Myofibrillar myopathies (MFMs) were proposed in 1996 as a group of chronic muscular disorders characterized by common morphologic features observed on muscle histology, which showed the focal dissolution of myofibrils followed by the accumulation of products of the degradative process.¹ The clinical phenotype of MFM is characterized by slowly progressive muscle weakness that can involve proximal or distal muscles, with onset in adulthood in most cases. However, other phenotypes are highly variable. Although 20% of patients with MFMs have been revealed to have mutations in *DES*, *CRYAB*, *MYOT*, *LDB (ZASP)*, *FLNC* or *BAG3*, the major genetic basis of MFMs remains to be elucidated.

Respiratory weakness is one of the symptoms of MFMs. The early or initial presentation of respiratory failure is not a common manifestation of MFMs as a whole, and there are limited reports regarding a fraction of patients with *DES*,² *MYOT*³ or *CRYAB*⁴ mutation. In 1993,

our group reported a Japanese family with dominantly inherited cytoplasmic body (CB) myopathy,⁵ which is now included in MFM. Currently, this family includes 20 patients in five successive generations who show almost homogeneous clinical features characterized by chronic progressive distal muscle weakness and early respiratory failure. However, the underlying genetic etiology in this family was unknown. The aim of this study was to determine the genetic cause in this family. To identify the responsible genetic mutation, we performed linkage analysis and whole-exome sequencing.

MATERIALS AND METHODS

This study was approved by the Ethics Committee of the Tohoku University School of Medicine, and all individuals gave their informed consent before their inclusion in the study.

¹Department of Medical Genetics, Tohoku University School of Medicine, Sendai, Japan; ²Department of Neurology, Tohoku University School of Medicine, Sendai, Japan; ³Department of Neurology and Division of Clinical Research, National Hospital Organization Nishitaga National Hospital, Sendai, Japan; ⁴Division of Cell Proliferation, United Centers for Advanced Research and Translational Medicine, Tohoku University Graduate School of Medicine, Sendai, Japan and ⁵Department of Neurology, Okayama University Medical School, Okayama, Japan

Correspondence: Dr Y Aoki, Department of Medical Genetics, Tohoku University School of Medicine, 1-1 Seiryō-machi, Aoba-ku, Sendai 980-8574, Japan.

E-mail: aokiy@med.tohoku.ac.jp

or Professor M Aoki, Department of Neurology, Tohoku University School of Medicine, 1-1 Seiryō-machi, Aoba-ku, Sendai 980-8574, Japan.

E-mail: aokim@med.tohoku.ac.jp

Received 23 October 2012; revised 9 January 2013; accepted 10 January 2013; published online 28 February 2013

Clinical information on the family

This family includes 20 patients (13 males and 7 females) in five successive generations (Figure 1). The family is of Japanese ancestry, and no consanguineous or international mating was found. Of all patients, seven underwent a muscle biopsy, and two were autopsied. All of the histological findings were compatible with MFM (see clinical data).

The age of onset ranged from 27–45 years. The most common presenting symptom was foot drop. At the initial evaluations, muscle weakness was primarily distributed in the ankle dorsiflexors and finger extensors. The patients were generally built and showed no other extramuscular abnormalities. In addition to this chronic progressive distal muscle weakness, respiratory distress occurred between 0 and 7 years from the initial onset (average 3.8 years) in seven patients (IV-9, V-2, A, B, E, H, and J) with adequate clinical information. Two patients who had not had any respiratory care died of respiratory failure approximately a decade from the initial onset. The other patients have been alive for more than 10 years (maximum 18 years) but require nocturnal non-invasive positive pressure ventilation. They were 37–58 years of age as of 2012 and able to walk independently with or without a simple walking aid. Although the time at which patients recognized dysphagia or dysarthria varied between 1 to more than 10 years from the initial onset, decreased bulbar functions had been noted at the initial evaluation in most cases. Cardiac function was normally maintained in all patients of the family.

Clinical data

The level of serum creatine kinase was normal or mildly elevated. Electromyography of affected muscles showed a chronic myogenic pattern, and the nerve conduction study did not suggest any neuropathic involvement. Muscle imaging showed focal atrophy in the tibialis anterior, tibialis posterior, extensor hallucis and digitorum longus, peroneal and semitendinosus muscle on initial assessment (Figure 2A), and atrophy became clear in cervical muscles, shoulder girdles, intercostals and proximal limb muscles in the following several years. Upon muscle biopsy, the most common finding was numerous cytoplasmic bodies (CBs), which were found on 7.3% of myofibers in the tibialis anterior of individual E (Figure 2B (a–c)) and 50–80% of intercostals in other cases.⁵

Other nonspecific findings were increased variability in the size of myofibers, central nuclei and rimmed vacuoles observed on a few fibers. No strong immunoreaction of desmin was seen in the CBs (Figure 2B (d, e)). An electron microscope examination showed that the regular sarcoplasmic pattern was replaced by abnormal fine filamentous structures, which seemed to attach to the Z-band. CBs were also found in almost all skeletal muscles and some smooth muscles in autopsied cases.⁵ Cardiac myofibers also contained numerous CBs in one of the autopsied cases (V-2),⁵ although the patient did not present any cardiac complication. The sequence analysis of the coding regions and flanking introns of *DES* and *MYOT* showed no pathogenic mutation in individual E. An array comparative genomic hybridization performed with the Agilent SurePrint G3 Human CGH 1M microarray format in individual A did not reveal any aberrations of genomic copy number.

Linkage analysis

DNA was extracted by standard methods. Linkage analysis was performed on nine family members (A–I in Figure 1; four of them were affected, and the others were unaffected) through genotyping using an Illumina Human Omni 2.5 BeadChip (Illumina, San Diego, CA, USA). We chose single-nucleotide polymorphisms (SNPs) that satisfied all of the following criteria: (1) autosomal SNPs whose allele frequencies were available from the HapMap project (<http://hapmap.ncbi.nlm.nih.gov/>), (2) SNPs that were not monomorphic among members and (3) SNPs that were not in strong linkage disequilibrium with neighboring SNPs (r^2 values <0.9). Then, we selected the first five SNPs from each position of integer genetic distance from SNPs that met the above criteria for the initial analysis. The details were as follows; we chose a SNP closest to 0 cM and the neighboring four SNPs. If the genetic distance of a SNP was the same as that of the next SNP, we considered the genomic position to determine their order. We repeated this process at 1 cM, 2 cM and so on.

We performed a multipoint linkage analysis of the data set (17 613 SNPs) using MERLIN⁶ 1.1.2 under the autosomal dominant mode with the following parameters: 0.0001 for disease allele frequency, 1.00 for individuals heterozygous and homozygous for the disease allele and 0.00 for individuals

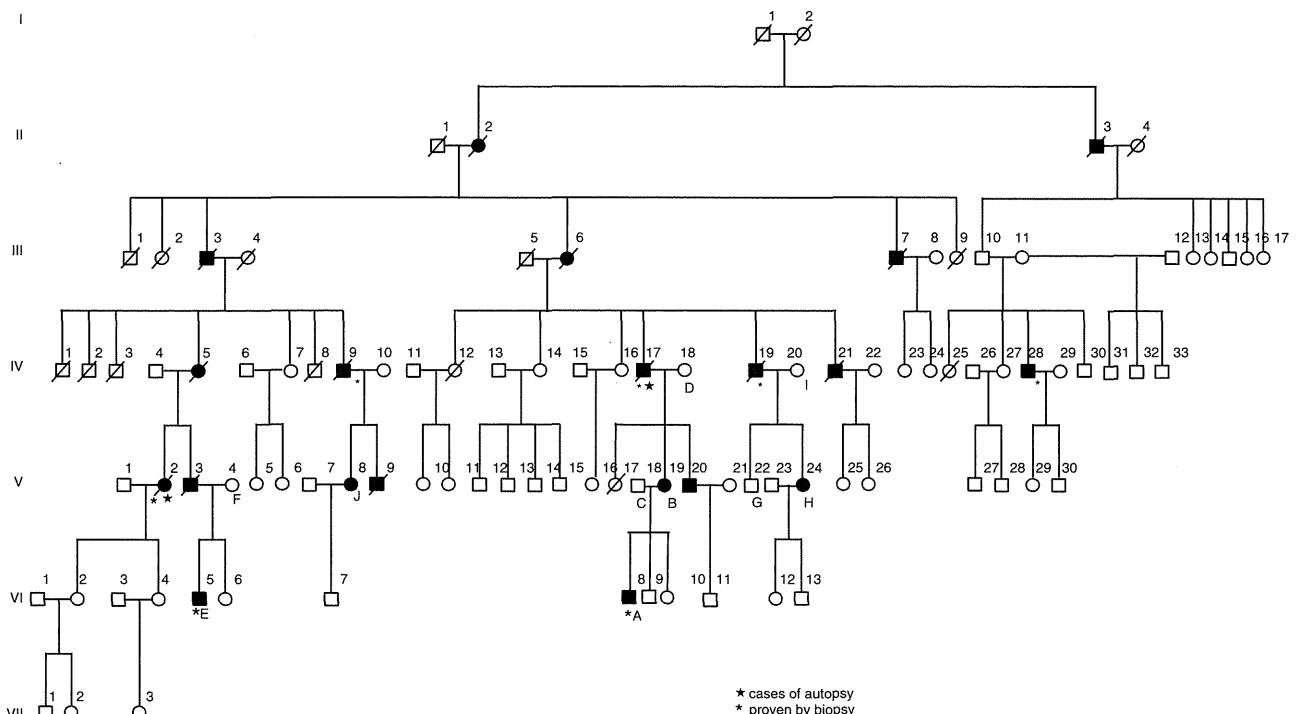


Figure 1 Family pedigree. Filled-in symbols indicate individuals with MFM. Empty symbols indicate unaffected individuals. A star and asterisk indicate autopsy-proven and muscle biopsy-proven cases, respectively. (A–J) indicates individuals whose DNA was used for this study.

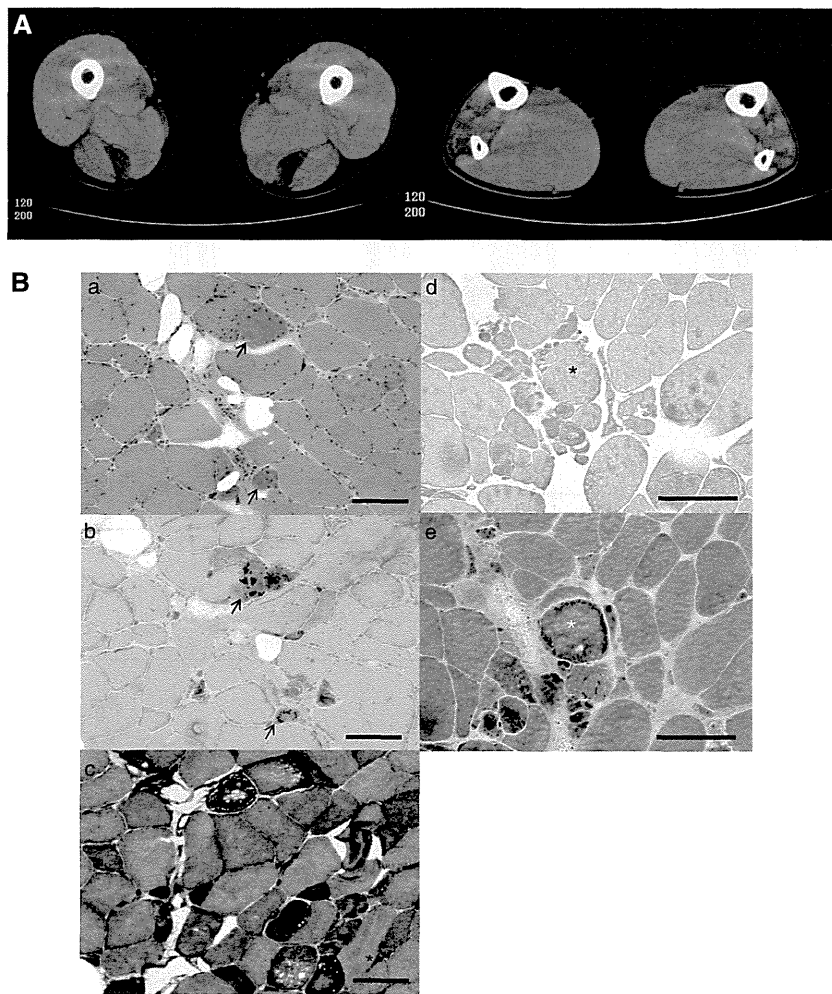


Figure 2 Family clinical data. **(A)** Muscle computed tomography of affected lower extremity. The imaging in the initial assessment of individual A showed symmetrical atrophy and fatty replacement of the semitendinosus in the proximal lower extremities (left) and the tibialis anterior, tibialis posterior, extensor hallucis and digitorum longus, and peroneal muscle in the distal (right) lower extremities. **(B)** Pathology of muscle biopsy. Hematoxylin-eosin (a), Gomori-trichrome (b) and NADH (nicotinamide adenine dinucleotide)-tetrazolium reductase (c) staining of the muscle biopsy sample from the tibialis anterior of individual E are shown. CBs are indicated by arrows. CBs were round or oval, 5–10 μm in diameter and predominantly located in the periphery of type 1 fibers, which stained eosinophilic with hematoxylin-eosin and blue-purple with Gomori-trichrome. NADH-tetrazolium reductase staining showed disorganization of the myofibrillar network. Immunostaining for desmin (d) and Gomori-trichrome staining (e) are serial sections of the muscle biopsy from individual E. Stars indicate corresponding fibers. No strong immunoreaction of desmin was seen in the CBs. Scale bars = 100 μm

homozygous for the alternative allele. After this first analysis, a second analysis was performed with all SNPs fulfilling the above criteria around the peaks identified in the first analysis.

Exome sequencing

Exome sequencing was performed on seven family members in three generations (A–E, H and I in Figure 1), four of whom were affected. Exon capture was performed with the SureSelect Human All Exon kit v2 (individuals E, H and I) or v4 (A–D) (Agilent Technologies, Santa Clara, CA, USA). Exon libraries were sequenced with the Illumina HiSeq 2000 platform according to the manufacturer's instructions (Illumina). Paired 101-base pair reads were aligned to the reference human genome (UCSCChG19) using the Burrows-Wheeler Alignment tool.⁷ Likely PCR duplicates were removed with the Picard program (<http://picard.sourceforge.net/>). Single-nucleotide variants and indels were identified using the Genome Analysis Tool Kit (GATK) v1.5 software.⁸ SNVs and indels were annotated against the RefSeq database and dbSNP135 with the ANNOVAR program.⁹ We used the PolyPhen2 polymorphism phenotyping software tool¹⁰ to predict the functional effects of mutations.

Sanger sequencing

To confirm that mutations identified by exome sequencing segregated with the disease, we performed direct sequencing. PCR was performed with the primers shown in Supplementary Table 1. PCR products were purified with a MultiScreen PCR plate (Millipore, Billerica, MA, USA) and sequenced using BigDye terminator v1.1 and a 3500xL genetic analyzer (Applied Biosystems, Carlsbad, CA, USA).

RESULTS

Linkage analysis

The first linkage analysis identified five regions across autosomes with a logarithm of odds (LOD) score greater than 2 (Figure 3). Of the five regions, two were on chromosome 2 (from 167 cM to 168 cM, with a maximum LOD score of 2.46 and from 182 cM to 185 cM, with a maximum LOD score of 2.71), the other two were on chromosome 8 (from 27 cM to 34 cM, with a maximum LOD score of 2.71 and at 61 cM, with a maximum LOD score of 2.03), and one was on

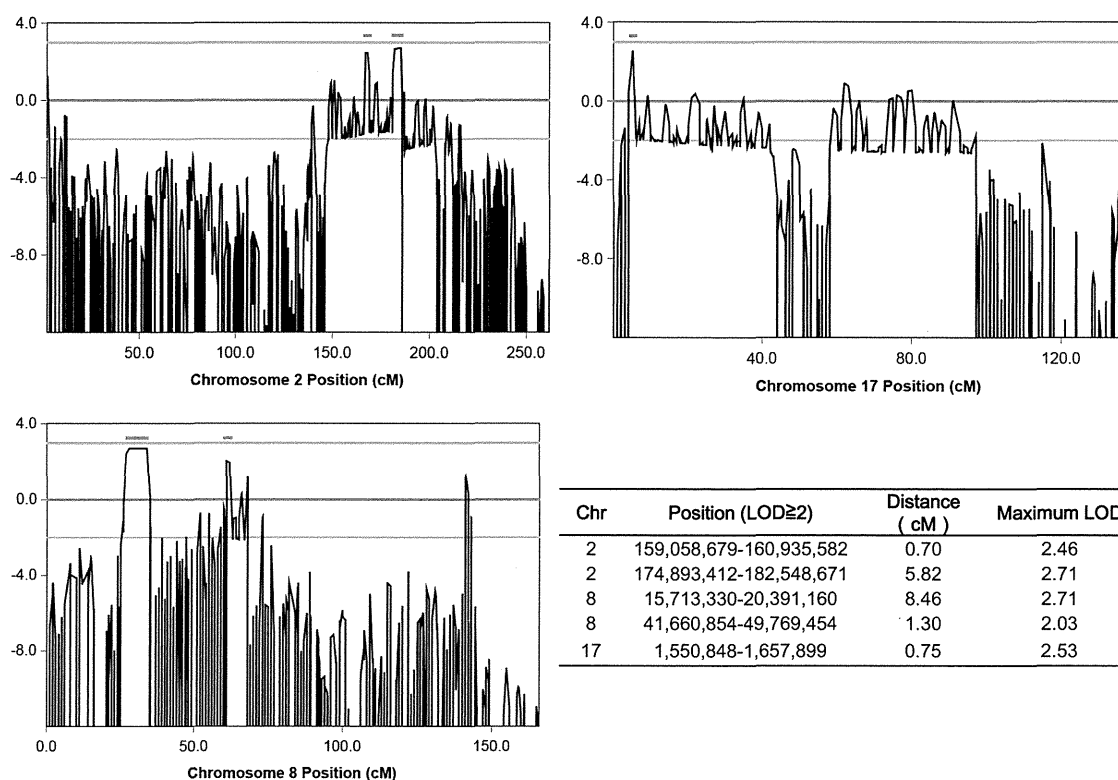


Figure 3 Linkage analysis. Linkage analysis was performed on nine family members (four of them were affected, the others were unaffected) using an Illumina Human Omni 2.5 BeadChip. Five regions with an LOD score greater than 2 (indicated by bar) were identified. A full color version of this figure is available at the *Journal of Human Genetics* journal online.

Table 1 Summary of detected variants by exome sequencing

Individual Morbidity	A Affected	B Affected	C Unaffected	D Unaffected	E Affected	H Affected	I Unaffected	Segregated in seven family members
Exonic, splicing	10 089	10 064	10 079	10 065	10 230	10 194	10 216	64
Nonsynonymous, splicing, indel, nonsense	4987	5020	5055	5038	5143	5234	5200	32
Allele frequency not available	577	600	536	555	671	794	786	2

chromosome 17 (at 5 cM, with a maximum LOD score of 2.53). In the second detailed linkage analysis, these peaks were determined to range from 167.49 cM at rs4233674 at position 159 058 679 to 168.19 cM at rs7598162 at position 160 935 582, and from 181.23 cM at rs4402725 at position 174 893 412 to 187.05 cM at rs7420169 at position 182 548 671 on chromosome 2; from 26.42 cM at rs2736043 at position 15 713 330 to 34.88 cM at rs9325871 at position 20 391 160, and from 61.02 cM at rs6999814 at position 41 660 854 to 62.32 cM at rs10957281 at position 49 769 454 on chromosome 8; and from 4.7 cM at rs11078552 at position 1 550 848 to 5.45 cM at rs1057355 at position 1 657 899 on chromosome 17. Haplotypes shared by affected individuals in these regions were confirmed by visual inspection. There were a few incompatible SNPs in these regions, presumably due to genotyping error.

Exome sequencing and segregation analysis

In exome sequencing, an average of 215 million reads enriched by SureSelect v4 (SSv4) and 319 million reads enriched by SureSelect v2 (SSv2) were generated, and 99% of reads were mapped to the

reference genome by Burrows-Wheeler Alignment tool. An average of 57% (SSv4) and 61% (SSv2) of those reads were duplicated and removed, and an average of 80% (SSv4) and 66% (SSv2) of mapped reads without duplicates were in target regions. The average coverage of each exome was 163-fold (SSv4) and 130-fold (SSv2). An average of 85% (SSv4) and 69% (SSv2) of target regions were covered at least 50-fold (Supplementary Table 2). On average, 10 133 SNVs or indels, which are located within coding exons or splice sites, were identified per individual (Table 1). A total of 64 variants were common among patients and not present in unaffected individuals, and 32 of those were left after excluding synonymous SNVs. In these variants, only the heterozygous mutation c.90263G>T (NM_001256850) at position 179 410 777 of chromosome 2, which was predicted to p.W30088L in *TTN*, was novel (that is, not present in dbSNP v135 or 1000 genomes). Polyphen2 predicted this mutation as probably damaging. This mutation was located in a candidate region suggested by the linkage analysis in the present study. The other variants were registered with dbSNP135, and the allele frequencies, except for one SNV, rs138183879, in *IKBKB*, ranged from 0.0023 to 0.62.

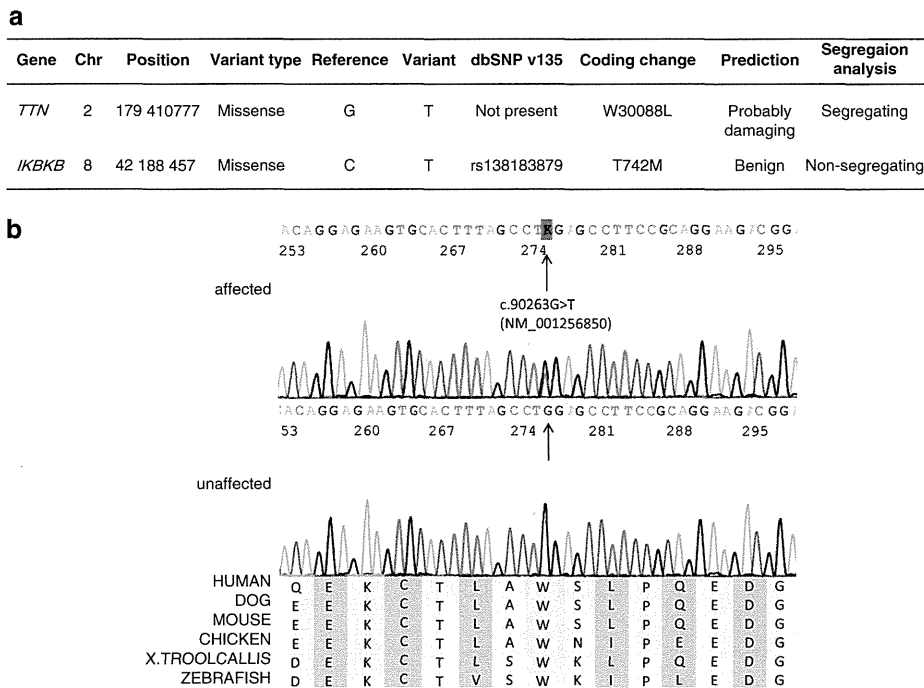


Figure 4 Identified mutations by exome sequencing. (a) We performed segregation analysis of two candidates. (b) The identified *TTN* mutation and its conservation among species. Sanger sequencing confirmed the heterozygous G to T substitution (indicated by the arrow) at the position chr2;179 410 777, which corresponds to c.90263G>T in exon 293 (NM_001256850.1). The substitution leads to p.W30088L (NP_001243779.1), and this amino acid is conserved among species.

These values were not compatible with the assumption that MFMs was a rare disease and showed complete penetrance in this family. The allele frequency of rs138183879 was not available in dbSNP135, and this SNV was in the candidate region on chromosome 8 based on linkage analysis.

We then performed a segregation analysis on the two candidates, the novel mutation c.90263G>T in *TTN* and rs138183879 in *IKBKB*, through Sanger sequencing in 10 family members (A–J in Figure 1; Figure 4a). The rs138183879 SNP was not found in individual J, that is, it was not segregated with the disease in this family. In contrast, the novel mutation c.90263G>T in *TTN* was detected in all patients ($n=5$) and not detected in any of the unaffected family members ($n=5$) or 191 ethnically matched control subjects (382 chromosomes). These results suggested that this rare mutation in *TTN* segregated with the disease in this family.

DISCUSSION

In this study, we found that a novel missense mutation in *TTN* segregated with MFM in a large Japanese family. The identified c.90263G>T mutation in *TTN* (NM_001256850) was considered to be the genetic cause of MFM in our family, because (1) exome sequencing revealed that this was the best candidate mutation after filtering SNPs and indels, (2) this mutation is located in a region on chromosome 2 shared by affected family members, (3) the segregation with MFM was confirmed by Sanger sequencing, (4) this mutation was not detected in 191 control individuals, (5) this mutation was predicted to alter highly conserved amino acids (Figure 4b) and (6) *TTN* encodes a Z-disc-binding molecule called titin, which is similar to all of the previously identified causative genes for MFMs, which also encode Z-disc-associated molecules.

Recently, three mutations in *TTN* have been reported as the causes of hereditary myopathy with early respiratory failure (HMERF,

MIM #603689),^{11–16} which has similar muscle pathology to MFMs. The identified novel missense mutation c.90263G>T in our study was located on the same exon as recently reported HMERF mutations: c.90272C>T in a Portuguese family¹⁶ and c.90315T>C in Swedish and English families^{14,15} (Table 2). This finding suggests the possibility that our family can be recognized as having HMERF from a clinical aspect.

Compared with symptoms described in the past three reports on HMERF (also see Table 2), our patients have common features, such as autosomal dominant inheritance, early respiratory failure, the absence of clinically apparent cardiomyopathy, normal to mild elevation of serum CK and histological findings compatible with MFM. Early involvement of the tibialis anterior is also common, except for the Portuguese family, who reported isolated respiratory insufficiency and a milder presentation of HMERF. Thus, our family shares major clinical manifestations with patients with HMERF, suggesting that the identified mutation is novel for MFM and HMERF.

To date, mutations in *TTN* have been identified in skeletal myopathy and cardiomyopathy.^{17,18} The relationship between the variant positions on *TTN* and phenotypes accompanied by skeletal or respiratory muscle involvement is summarized in Table 2. Titin is a large protein (4.20 MDa) that extends from the Z-disk to the M-line within the sarcomere, and it is composed of four major domains: Z-disc, I-band, A-band and M-line (Figure 5). All four HMERF mutations detected by other groups and our study were consistently located in the A-band domain, while mutations in tibial muscular dystrophy (TMD) (MIM #600334),^{19–24} limb-girdle muscular dystrophy type 2J (LGMD2J) (#608807)^{19,25} and early-onset myopathy with fatal cardiomyopathy (#611705)²⁶ were located in the M-line domain. HMERF and TMD have some common clinical characteristics, such as autosomal dominant inheritance with onset in adulthood and strong involvement of the tibialis anterior muscle.

Table 2 Previously reported TTN mutations with skeletal and/or respiratory muscle involvement

Phenotype	LGMD	HMERF	Our family	HMERF	HMERF	TMD	TMD	LGMD2J	TMD	TMD	TMD	TMD	TMD	Early-onset	Early-onset
														with fatal	with fatal
														cardiomyopathy	cardiomyopathy
Reported by	Vasli et al. ¹⁶	Ohlsson et al. ¹⁴ Pfeffer et al. ¹⁵	Abe et al. ⁵	Vasli et al. ¹⁶	Edstrom et al. ¹² Nicolao, et al. ¹¹ Lang e et al. ¹³ 2005	Hackman et al. ²³	Udd et al. ²⁰ Hackman et al. ¹⁹	Udd et al. ²⁵ Hackman et al. ¹⁹	Pollazzon et al. ²⁴	Van den Bergh et al. ²²	Seze et al. ²¹ Hackman et al. ¹⁹	Hackman et al. ²³	Hackman et al. ²³	Carmignac et al. ²⁶	Carmignac et al. ²⁶
Mutation identified in Nucleotide (NM_001256850.1)	2012 c.3100G>A, c.52024G>A	2012 c.90315T>C	2012 c.90263G>T	2012 c.90272C>T	c.97348C>T	2008 c.102724delT	2002 102857_102867 del11ins11	2002 102857_102867 del11ins11	2010 c.102914A>C	2003 c.102917T>A	2002 c.102944T>C	2008. c.102966delA	2008 c.102967C>T	2007 g.289385del ACCAAGTG	2007 g.291297delA
Protein (NP_001243779.1) Domain	p.V1034M, p.A17342T I-band, A-band	p.C30071R A-band (Fn3)	p.W30088L A-band (Fn3)	p.P30091L A-band (Fn3)	p.R32450W A-band (kinase) Swedish AD	M-line	M-line	M-line	M-line	M-line	M-line	M-line	M-line	M-line	M-line
Population Inheritance	French AR	Swedish English AD	Japanese AD	Portuguese AD	Swedish AD	French AD	Finnish AD	Finnish AR	Italian AD	Belgian AD	French AD	Spanish AD	French AD	Sudanese Consanguineous siblings Neonatal	Moroccan Consanguineous siblings Infant-early childhood
Onset	35	33–71	27–45	46	20–50s	20–30s	35–55	20–30s	50–60s	47	45	40–50s	30s		
Skeletal muscles															
Major	Proximal UL and LL	TA, PL, EDL, ST	TA, ST	No	TA, neck flexor, proximals	TA, GA,HAM, pelvic	TA	All proximals	TA	TA	TA	TA	TA, HAM, pelvic	General muscle weakness and hypotonia	Psoas, TA, GA, peroneus
Minor		Neck flexor	Cervical, shoulder girdles, intercostals, proximal limb	Facial		QF				EDL, peroneal, TP	GA, femoral, scapular	HAM, GA	GA, distal UL		QF, proximal UL, neck, facial, trunk flexor
Spared						Proximal UL	Facial, UL, proximals	Facial			UL, proximal LL	Facial	UL	Proximal UL, QF	
Cardiac muscles	ND	No	No	ND	ND	ND	No	No	ND	ND	ND	ND	ND	DCM, onset; in the first decade	DCM, onset; 5–12 years old
Respiratory failure	ND	Yes, within 5–8 years	Yes, within 7 years	Isolated respiratory failure	Yes, as first presentation	ND	ND	ND	ND	ND	ND	ND	ND	ND	ND
Muscle pathologic features	ND	Inclusion bodies (major) and RVs (minor)	Cytoplasmic bodies (major) and RVs (minor)	Cytoplasmic bodies	Cytoplasmic bodies, positive for rhodamine-conjugated phalloidin	Dystrophic pattern without vacuoles	Nonspecific dystrophic change	Nonspecific dystrophic change, loss of calpain-3	Dystrophic pattern with RVs	Nonspecific, RV	Nonspecific	Dystrophic pattern with RVs	Nonspecific	Minicore-like lesions and abundant central nuclei	Minicore-like lesions and abundant central nuclei

Abbreviations: AD, autosomal dominant; AR, autosomal recessive; DCM, dilated cardiomyopathy; EDL, extensor digitorum longus; GA, gastrocnemius; HAM, hamstrings; LL, lower limb; ND, not described; no, no involvement; PL, peroneus longus; QF, quadriceps femoris; RV, rimmed vacuole; ST, semitendinosus; TA, tibialis anterior; TMD, tibial muscular dystrophy; TP, tibialis posterior; UL, upper limb.

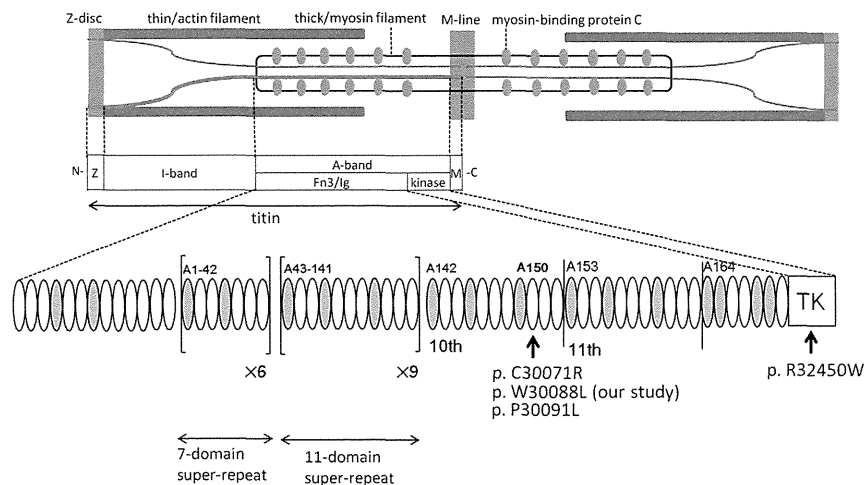


Figure 5 Structure of titin and mutation distribution in the A-band domain. Human *TTN* was mapped to 2q31.2. *TTN* is 294 kb and is composed of 363 exons that code for a maximum of 38 138 amino-acid residues and a 4.20-MDa protein³² called titin. Titin is expressed in the cardiac and skeletal muscles and spans half the sarcomere, with its N-terminal at the Z-disc and the C-terminal at the M-line.³³ Titin is composed of four major domains: Z-disc, I-band, A-band and M-line. I-band regions of titin are thought to make elastic connections between the thick filament (that is, myosin filament) and the Z-disc within the sarcomere, whereas the A-band domain of titin seems to be bound to the thick filament, where it may regulate filament length and assembly.³⁴ The gray and white ellipses indicate an Ig-like domain and fibronectin type 3 domain, respectively. Our mutation (p.W30088L) and the neighboring two mutations (that is, p.C30071R and p.P30091L) were all located in the 6th Fn3 domain in the 10th domain of large super-repeats. A full color version of this figure is available at the *Journal of Human Genetics* journal online.

In contrast, one of the distinctive features of TMD is that early respiratory failure has not been observed in patients with TMD. Histological findings of TMD usually do not include CBs but show nonspecific dystrophic change. The underlying pathogenic processes explaining why mutations on these neighboring domains share some similarities but also some differences are unknown.

Three of four HMERF mutations in the A-band domain are located in the fibronectin type 3 and Ig-like (Fn3/Ig) domain, and one of four HMERF mutations is located in the kinase domain (Table 2, also see Figure 5). The missense mutation c.97348C>T in the kinase domain was the first reported HMERF mutation. It has been shown that the kinase domain has an important role in controlling muscle gene expression and protein turnover via the neighbor of BRCA1 gene-1-muscle-specific RING finger protein-serum response transcription factor pathway.¹³ Moreover, the Fn3/Ig domain is composed of two types of super-repeats: six consecutive copies of 7-domain super-repeat at the N-terminus and 11 consecutive copies of 11-domain super-repeat at the C-terminus.^{27–29} These super-repeats are highly conserved among species and muscles. Our identified mutation (c.90263G>T) and the neighboring two mutations (that is, c.90272C>T and c.90315T>C shown in Table 2) were all located on the 6th Fn3 domain in the 10th copy of 11-domain super-repeat (that is, A150 domain³⁰) (Figure 5). Although some Fn3 domains are proposed to be the putative binding site for myosin,³¹ the role with the majority of Fn3 domains, how it supports the structure of each repeat architecture, and the identity of its binding partner have not been fully elucidated. Our findings suggested that the Fn3 domain, in which mutations clustered, has critical roles in the pathogenesis of HMERF, although detailed mechanisms of pathogenesis remain unknown.

In conclusion, we have identified a novel disease-causing mutation in *TTN* in a family with MFEM that was clinically compatible with HMERF. Because of its large size, global mutation screening of *TTN* has been difficult. Mutations in *TTN* may be detected by massively parallel sequencing in more patients with MFEMs, especially in patients with early respiratory failure. Further studies are needed to

understand the genotype–phenotype correlations in patients with mutations in *TTN* and the molecular function of titin.

ACKNOWLEDGEMENTS

We thank the patients and their family. We are grateful to Yoko Tateda, Kumi Kato, Naoko Shimakura, Risa Ando, Riyo Takahashi, Miyuki Tsuda, Nozomi Koshita, Mami Kikuchi and Kiyotaka Kuroda for their technical assistance. We also acknowledge the support of the Biomedical Research Core of Tohoku University Graduate School of Medicine. This work was supported by a grant of Research on Applying Health Technology provided by the Ministry of Health, Labor and Welfare to YM, an Intramural Research Grant (23-5) for Neurological and Psychiatric Disorders of NCNP and JSPS KAKENHI Grant number 24659421.

- 1 Nakano, S., Engel, A. G., Waclawik, A. J., Emslie-Smith, A. M. & Busis, N. A. Myofibrillar myopathy with abnormal foci of desmin positivity. I. Light and electron microscopy analysis of 10 cases. *J. Neuropathol. Exp. Neurol.* **55**, 549–562 (1996).
- 2 Olive, M., Odgerel, Z., Martinez, A., Poza, J. J., Bragado, F. G., Zabalza, R. J. *et al.* Clinical and myopathological evaluation of early- and late-onset subtypes of myofibrillar myopathy. *Neuromuscul. Disord.* **21**, 533–542 (2011).
- 3 Olive, M., Goldfarb, L. G., Shatunov, A., Fischer, D. & Ferrer, I. Myotilinopathy: refining the clinical and myopathological phenotype. *Brain* **128**, 2315–2326 (2005).
- 4 Selcen, D. & Engel, A. G. Myofibrillar myopathy caused by novel dominant negative alpha B-crystallin mutations. *Ann. Neurol.* **54**, 804–810 (2003).
- 5 Abe, K., Kobayashi, K., Chida, K., Kimura, N. & Kogure, K. Dominantly inherited cytoplasmic body myopathy in a Japanese kindred. *Tohoku. J. Exp. Med.* **170**, 261–272 (1993).
- 6 Abecasis, G. R., Cherny, S. S., Cookson, W. O. & Cardon, L. R. Merlin—rapid analysis of dense genetic maps using sparse gene flow trees. *Nat. Genet.* **30**, 97–101 (2002).
- 7 Li, H. & Durbin, R. Fast and accurate short read alignment with Burrows-Wheeler transform. *Bioinformatics* **25**, 1754–1760 (2009).
- 8 McKenna, A., Hanna, M., Banks, E., Sivachenko, A., Cibulskis, K., Kernysky, A. *et al.* The Genome Analysis Toolkit: a MapReduce framework for analyzing next-generation DNA sequencing data. *Genome. Res.* **20**, 1297–1303 (2010).
- 9 Wang, K., Li, M. & Hakonarson, H. ANNOVAR: functional annotation of genetic variants from high-throughput sequencing data. *Nucleic Acids Res.* **38**, e164 (2010).
- 10 Adzhubei, I. A., Schmidt, S., Peshkin, L., Ramensky, V. E., Gerasimova, A., Bork, P. *et al.* A method and server for predicting damaging missense mutations. *Nat. Methods* **7**, 248–249 (2010).
- 11 Nicolao, P., Xiang, F., Gunnarsson, L. G., Giometto, B., Edstrom, L., Anvret, M. *et al.* Autosomal dominant myopathy with proximal weakness and early respiratory muscle involvement maps to chromosome 2q. *Am. J. Hum. Genet.* **64**, 788–792 (1999).

- 12 Edstrom, L., Thornell, L. E., Albo, J., Landin, S. & Samuelsson, M. Myopathy with respiratory failure and typical myofibrillar lesions. *J. Neurol. Sci.* **96**, 211–228 (1990).
- 13 Lange, S., Xiang, F., Yakovenko, A., Vihola, A., Hackman, P., Rostkova, E. *et al.* The kinase domain of titin controls muscle gene expression and protein turnover. *Science* **308**, 1599–1603 (2005).
- 14 Ohlsson, M., Hedberg, C., Bradvik, B., Lindberg, C., Tajsharghi, H., Danielsson, O. *et al.* Hereditary myopathy with early respiratory failure associated with a mutation in A-band titin. *Brain* **135**, 1682–1694 (2012).
- 15 Pfeffer, G., Elliott, H. R., Griffin, H., Barresi, R., Miller, J., Marsh, J. *et al.* Titin mutation segregates with hereditary myopathy with early respiratory failure. *Brain* **135**, 1695–1713 (2012).
- 16 Vasli, N., Bohm, J., Le Gras, S., Muller, J., Pizot, C., Jost, B. *et al.* Next generation sequencing for molecular diagnosis of neuromuscular diseases. *Acta Neuropathol.* **124**, 273–283 (2012).
- 17 Kontogianni-Konstantopoulos, A., Ackermann, M. A., Bowman, A. L., Yap, S. V. & Bloch, R. J. Muscle giants: molecular scaffolds in sarcomerogenesis. *Physiol. Rev.* **89**, 1217–1267 (2009).
- 18 Ottenheijm, C. A. & Granzier, H. Role of titin in skeletal muscle function and disease. *Adv. Exp. Med. Biol.* **682**, 105–122 (2010).
- 19 Hackman, P., Vihola, A., Haravuori, H., Marchand, S., Sarparanta, J., De Seze, J. *et al.* Tibial muscular dystrophy is a titinopathy caused by mutations in TTN, the gene encoding the giant skeletal-muscle protein titin. *Am. J. Hum. Genet.* **71**, 492–500 (2002).
- 20 Udd, B., Partanen, J., Halonen, P., Falck, B., Hakamies, L., Heikkila, H. *et al.* Tibial muscular dystrophy. Late adult-onset distal myopathy in 66 Finnish patients. *Arch. Neurol.* **50**, 604–608 (1993).
- 21 de Seze, J., Udd, B., Haravuori, H., Sablonniere, B., Maurage, C. A., Hurtevent, J. F. *et al.* The first European family with tibial muscular dystrophy outside the Finnish population. *Neurology* **51**, 1746–1748 (1998).
- 22 Van den Bergh, P. Y., Bouquiaux, O., Verellen, C., Marchand, S., Richard, I., Hackman, P. *et al.* Tibial muscular dystrophy in a Belgian family. *Ann. Neurol.* **54**, 248–251 (2003).
- 23 Hackman, P., Marchand, S., Sarparanta, J., Vihola, A., Penisson-Besnier, I., Eymard, B. *et al.* Truncating mutations in C-terminal titin may cause more severe tibial muscular dystrophy (TMD). *Neuromuscul. Disord.* **18**, 922–928 (2008).
- 24 Pollazzon, M., Suominen, T., Penttila, S., Malandrini, A., Carluccio, M. A., Mondelli, M. *et al.* The first Italian family with tibial muscular dystrophy caused by a novel titin mutation. *J. Neurol.* **257**, 575–579 (2010).
- 25 Udd, B., Rapola, J., Nokelainen, P., Arikawa, E. & Somer, H. Nonvacuolar myopathy in a large family with both late adult onset distal myopathy and severe proximal muscular dystrophy. *J. Neurol. Sci.* **113**, 214–221 (1992).
- 26 Carmignac, V., Salih, M. A., Quijano-Roy, S., Marchand, S., Al Rayess, M. M., Mukhtar, M. M. *et al.* C-terminal titin deletions cause a novel early-onset myopathy with fatal cardiomyopathy. *Ann. Neurol.* **61**, 340–351 (2007).
- 27 Labeit, S., Barlow, D. P., Gautel, M., Gibson, T., Holt, J., Hsieh, C. L. *et al.* A regular pattern of two types of 100-residue motif in the sequence of titin. *Nature* **345**, 273–276 (1990).
- 28 Labeit, S. & Kolmerer, B. Titins: giant proteins in charge of muscle ultrastructure and elasticity. *Science* **270**, 293–296 (1995).
- 29 Tskhovrebova, L., Walker, M. L., Grossmann, J. G., Khan, G. N., Baron, A. & Trinick, J. Shape and flexibility in the titin 11-domain super-repeat. *J. Mol. Biol.* **397**, 1092–1105 (2010).
- 30 Bucher, R. M., Svergun, D. I., Muhle-Goll, C. & Mayans, O. The structure of the FnIII Tandem A77-A78 points to a periodically conserved architecture in the myosin-binding region of titin. *J. Mol. Biol.* **401**, 843–853 (2010).
- 31 Muhle-Goll, C., Habeck, M., Cazorla, O., Nilges, M., Labeit, S. & Granzier, H. Structural and functional studies of titin's fn3 modules reveal conserved surface patterns and binding to myosin S1—a possible role in the Frank-Starling mechanism of the heart. *J. Mol. Biol.* **313**, 431–447 (2001).
- 32 Bang, M. L., Centner, T., Fornoff, F., Geach, A. J., Gotthardt, M., McNabb, M. *et al.* The complete gene sequence of titin, expression of an unusual approximately 700-kDa titin isoform, and its interaction with obscurin identify a novel Z-line to I-band linking system. *Circ. Res.* **89**, 1065–1072 (2001).
- 33 Maruyama, K., Yoshioka, T., Higuchi, H., Ohashi, K., Kimura, S. & Natori, R. Connectin filaments link thick filaments and Z lines in frog skeletal muscle as revealed by immunoelectron microscopy. *J. Cell. Biol.* **101**, 2167–2172 (1985).
- 34 Guo, W., Bharmal, S. J., Esbona, K. & Greaser, M. L. Titin diversity—alternative splicing gone wild. *J. Biomed. Biotechnol.* **2010**, 753675 (2010).

Supplementary Information accompanies the paper on Journal of Human Genetics website (<http://www.nature.com/jhg>)

Gain-of-Function Mutations in *RIT1* Cause Noonan Syndrome, a RAS/MAPK Pathway Syndrome

Yoko Aoki,^{1,*} Tetsuya Niihori,¹ Toshihiro Banjo,² Nobuhiko Okamoto,³ Seiji Mizuno,⁴ Kenji Kurosawa,⁵ Tsutomu Ogata,⁶ Fumio Takada,⁷ Michihiro Yano,⁸ Toru Ando,⁹ Tadataka Hoshika,¹⁰ Christopher Barnett,^{11,12} Hirofumi Ohashi,¹³ Hiroshi Kawame,¹⁴ Tomonobu Hasegawa,¹⁵ Takahiro Okutani,¹⁶ Tatsuo Nagashima,¹⁷ Satoshi Hasegawa,¹⁸ Ryo Funayama,¹⁹ Takeshi Nagashima,¹⁹ Keiko Nakayama,¹⁹ Shin-ichi Inoue,¹ Yusuke Watanabe,² Toshihiko Ogura,² and Yoichi Matsubara^{1,20}

RAS GTPases mediate a wide variety of cellular functions, including cell proliferation, survival, and differentiation. Recent studies have revealed that germline mutations and mosaicism for classical RAS mutations, including those in *HRAS*, *KRAS*, and *NRAS*, cause a wide spectrum of genetic disorders. These include Noonan syndrome and related disorders (RAS/mitogen-activated protein kinase [RAS/MAPK] pathway syndromes, or RASopathies), nevus sebaceous, and Schimmelpenning syndrome. In the present study, we identified a total of nine missense, nonsynonymous mutations in *RIT1*, encoding a member of the RAS subfamily, in 17 of 180 individuals (9%) with Noonan syndrome or a related condition but with no detectable mutations in known Noonan-related genes. Clinical manifestations in the *RIT1*-mutation-positive individuals are consistent with those of Noonan syndrome, which is characterized by distinctive facial features, short stature, and congenital heart defects. Seventy percent of mutation-positive individuals presented with hypertrophic cardiomyopathy; this frequency is high relative to the overall 20% incidence in individuals with Noonan syndrome. Luciferase assays in NIH 3T3 cells showed that five *RIT1* alterations identified in children with Noonan syndrome enhanced ELK1 transactivation. The introduction of mRNAs of mutant *RIT1* into 1-cell-stage zebrafish embryos was found to result in a significant increase of embryos with craniofacial abnormalities, incomplete looping, a hypoplastic chamber in the heart, and an elongated yolk sac. These results demonstrate that gain-of-function mutations in *RIT1* cause Noonan syndrome and show a similar biological effect to mutations in other RASopathy-related genes.

RAS GTPases are monomeric G proteins with a molecular mass of 20–40 kDa and cycle between a GTP-bound active and a GDP-bound inactive state. The members of the RAS superfamily are structurally classified into at least five subfamilies: RAS, Rho, Rab, Sar1/Arf, and Ran families.^{1,2} The Ras subfamily consists of classical RAS proteins (*HRAS*, *KRAS*, and *NRAS*), *RRAS*, *RRAS2* (*TC21*), *RRAS3* (*MRAS*), *RAPs*, *RAEB*, *RALs*, *RIT1*, and *RIT2* (*RIN*). RAS proteins interact with multiple effectors, including RAF kinases, phosphatidylinositol 3-kinase (PI-3 kinase), *RalGDS*, *p120GAP*, *MEKK1*, *RIN1*, *AF-6*, phospholipase C epsilon, and the Nore-MST1 complex, and activate multiple downstream signaling cascades.^{1,2} Of these signaling pathways, the RAS/mitogen-activated protein kinase (RAS/MAPK) signaling pathway plays a central role in cellular proliferation and differentiation.

Noonan syndrome (MIM 163950) is an autosomal-dominant disorder characterized by short stature, distinctive facial features, and congenital heart defects.^{3,4} The distinctive facial features include hypertelorism, downslanting palpebral fissures, ptosis, a webbed or short neck, and low-set, posteriorly rotated ears. Congenital heart defects, including pulmonary valve stenosis and atrial septal defects, occur in 50%–80% of individuals. Hypertrophic cardiomyopathy is observed in 20% of affected individuals. Other clinical manifestations include cryptorchidism, mild intellectual disability, bleeding tendency, and hydrops fetalis. The incidence of this syndrome is estimated to be between 1 in 1,000 to 1 in 2,500 live births. Individuals with Noonan syndrome are at risk of juvenile myelomonocytic leukemia (JMML), a myeloproliferative disorder characterized by excessive production of myelomonocytic cells.⁴ Noonan syndrome exhibits phenotypic overlap

¹Department of Medical Genetics, Tohoku University School of Medicine, Sendai 980-8574, Japan; ²Department of Developmental Neurobiology, Institute of Development, Aging, and Cancer, Tohoku University, Sendai 980-8575, Japan; ³Department of Medical Genetics, Osaka Medical Center and Research Institute for Maternal and Child Health, Izumi 594-1101, Japan; ⁴Department of Pediatrics, Central Hospital, Aichi Human Service Center, Kasugai 480-0392, Japan; ⁵Division of Medical Genetics, Kanagawa Children's Medical Center, Yokohama 232-8555, Japan; ⁶Department of Pediatrics, Hamamatsu University School of Medicine, Hamamatsu 431-3192, Japan; ⁷Department of Medical Genetics, Kitasato University Graduate School of Medical Sciences, Sagami-hara 252-0373, Japan; ⁸Department of Pediatrics, Akita University School of Medicine, Akita 010-8543, Japan; ⁹Department of Pediatrics, Municipal Tsuruga Hospital, Tsuruga 914-8502, Japan; ¹⁰Department of Pediatrics, Tottori Prefectural Central Hospital, Tottori 680-0901, Japan; ¹¹South Australian Clinical Genetics Service, SA Pathology, Women's and Children's Hospital, North Adelaide, Adelaide, SA 5006, Australia; ¹²School of Paediatrics and Reproductive Health, University of Adelaide, Adelaide, SA 5005, Australia; ¹³Division of Medical Genetics, Saitama Children's Medical Center, Saitama 339-8551, Japan; ¹⁴Department of Genetic Counseling, Ochanomizu University, Tokyo 112-8610, Japan; ¹⁵Department of Pediatrics Keio University School of Medicine, Tokyo 160-8582, Japan; ¹⁶Division of Neonatal Intensive Care Unit, General Perinatal Medical Center, Wakayama Medical University, Wakayama 641-8510, Japan; ¹⁷Department of Pediatrics, Jikei University School of Medicine, Tokyo 105-8461, Japan; ¹⁸Department of Pediatrics, Niigata Graduate School of Medical and Dental Sciences, Niigata 951-8510, Japan; ¹⁹Division of Cell Proliferation, United Centers for Advanced Research and Translational Medicine, Tohoku University Graduate School of Medicine, Sendai 980-8575, Japan; ²⁰National Research Institute for Child Health and Development, Tokyo 157-8535, Japan

*Correspondence: aoki@med.tohoku.ac.jp

<http://dx.doi.org/10.1016/j.ajhg.2013.05.021>. ©2013 by The American Society of Human Genetics. All rights reserved.

with Costello syndrome (MIM 218040) and cardiofaciocutaneous (CFC) syndrome (MIM 115150).

In 2001, Tartaglia et al. identified missense mutations in protein-tyrosine phosphatase, nonreceptor type 11 (*PTPN11* [MIM 176876]), which encodes the tyrosine phosphatase SHP-2 in 50% of individuals with Noonan syndrome.⁵ In contrast, loss-of-function or dominant-negative mutations in *PTPN11* have been reported in individuals with Noonan syndrome with multiple lentigines⁶ (formerly referred to as LEOPARD [multiple lentigines, electrocardiographic conduction abnormalities, ocular hypertelorism, pulmonic stenosis, abnormal genitalia, retardation of growth, and sensorineural deafness] syndrome [MIM 151100]). To date, germline mutations in *PTPN11*, *KRAS* (MIM 190070), *SOS1* (MIM 182530), *RAF1* (MIM 164760), and *NRAS* (MIM 164790) have been identified in individuals with Noonan syndrome^{7–12} (NS1 [MIM 163950], NS3 [MIM 609942], NS4 [MIM 610733], NS5 [MIM 611553], and NS6 [MIM 613224]), and mutations in *SHOC2* (MIM 602775) and *CBL* (MIM 165360) have been identified in two Noonan-syndrome-like syndromes^{13–16} (NSLH [MIM 607721] and NSLL [MIM 613563], respectively) (Figure S1, available online). Moreover, we and another group have identified germline mutations in *HRAS* (MIM 190020) in individuals with Costello syndrome¹⁷ and germline mutations in *KRAS*, *BRAF* (MIM 164757), *MAP2K1* (MIM 176872), and *MAP2K2* (MIM 601263) in individuals with CFC syndrome.^{18,19} Mutations in *BRAF* have been also identified in a small percentage of individuals with Noonan syndrome (NS7 [MIM 613706]). A line of studies have shown that a group of the above genetic disorders result from dysregulation of the RAS and downstream signaling cascade (RAS/MAPK pathway syndromes, or RASopathies).^{20,21} Recently, mosaicism for *KRAS* and *HRAS* mutations has been reported in nevus sebaceous and Schimmelpenning syndrome,²² further extending a spectrum of diseases with a dysregulated RAS/MAPK pathway.

To identify genetic causes of Noonan syndrome, we recruited 180 individuals with Noonan syndrome or a related phenotype; they were negative for all coding exons in *PTPN11*, *KRAS*, *HRAS*, and *SOS1*; exons 6 and 11–16 in *BRAF*; exons 7, 14, and 17 in *RAF1*; exons 2 and 3 in *MAP2K1* and *MAP2K2*; and exon 1 in *SHOC2*. Further genetic analysis has been conducted according to their first diagnoses.^{17,23–29} This study was approved by the ethics committee of Tohoku University School of Medicine. We obtained informed consent from all subjects involved in the study. We sequenced the exomes of 14 individuals whose clinical manifestations had been confirmed to be consistent with Noonan syndrome by trained dysmorphologists. Targeted enrichment was performed with the Agilent SureSelect Human All Exon v.1 Kit for four individuals and with the SureSelect Human All Exon 50Mb kit for ten individuals. Exon-enriched DNA libraries from these 14 individuals were sequenced on the Illumina HiSeq 2000 for 91 bp (v.1 kit) or 101 bp (50Mb kit). The

Burrows-Wheeler Aligner (BWA) was used to align the sequence reads to the human genome (UCSC Genome Browser hg19);³⁰ all BWA parameters were kept at the default settings. After the removal of duplicates from the alignments, realignment around known indels, recalibration, and SNP and indel calling were performed with the Genome Analysis Toolkit (v.1.5).³¹ ANNOVAR was used for annotation against the RefSeq database and dbSNP.³² We identified approximately 10,000 nonsynonymous, nonsense, and splice-site variations and coding indels per individual (Table S1). Filtering steps using variant databases (dbSNP132 and the 1000 Genome Project database) and in-house exome data were carried out, resulting in the identification of 122–282 variants per individual. By visual inspection of the generated data, four heterozygous *RIT1* (MIM 609591; RefSeq accession number NM_006912.5) variants (c.246T>G [p.Phe82Leu], c.265T>C [p.Tyr89His], c.270G>T [p.Met90Ile], and c.284G>C [p.Gly95Ala]) were found in four individuals. Sanger sequencing validated the heterozygous state of the four variants. We did not find any other strong candidate genes in the results of exome sequencing.

RIT1 shares approximately 50% sequence identity with RAS, has an additional N-terminal extension, and does not possess a C-terminal CAAX motif, a specific motif for post-translational modification.^{33,34} *RIT1* is located in chromosomal region 1q22 and consists of six exons. We analyzed an additional 166 individuals diagnosed with Noonan syndrome or a related disorder but without mutations in known genes.^{17,23–29} Sanger sequencing of all coding exons in *RIT1* in the 166 individuals showed that 13 in 166 individuals had changes. Combining with the 4 in 14 individuals from exome sequencing, a total of nine missense, nonsynonymous mutations were identified in 17 of 180 (9%) individuals who were suspected to have Noonan syndrome or a related disorder (Table 1 and Figures 1A–1L). The identified germline *RIT1* mutations encode alterations located in the G1 domain (c.104G>C [p.Ser35Thr]); the switch I region, involving the G2 domain (c.170C>G [p.Ala57Gly]); and the switch II region, corresponding to RAS (c.242A>G [p.Glu81Gly], c.244T>G [p.Phe82Val], c.246T>G [p.Phe82Leu], c.247A>C [p.Thr83Pro], c.265T>C [p.Tyr89His], c.270G>T [p.Met90Ile], and c.284G>C [p.Gly95Ala]) (Figure S2). Amino acids where alterations are located are conserved among species (Figure S3). The *RIT1* mutations encode alterations clustered in the switch II region. In contrast, *HRAS* germline mutations identified in Costello syndrome are clustered at codon 12 and 13 in the region encoding the G1 domain¹⁷ (Figure 1M). Mutations in parents were not identified in seven families. These mutations are apparently de novo, but biologic confirmation of parentage was not performed. One mutation, c.104G>C, was inherited from a mother with a Noonan syndrome phenotype (Table 1). None of these mutations were identified in 480 controls.

To assess the functional consequences of *RIT1* mutations identified in affected individuals, we introduced a

Table 1. Mutations in *RIT1*, Family Status, and Heart Defects of Mutation-Positive Individuals

Subject	Exon	Nucleotide Change ^a	Amino Acid Change ^b	Father	Mother	HCM ^c	PS ^c	Other Heart Defects ^c
NS414	2	c.104G>C	p.Ser35Thr	WT	p.Ser35Thr	+	-	MVP, MR
KCC27	2	c.104G>C	p.Ser35Thr	NA	NA	+	+	-
NS43	4	c.170C>G	p.Ala57Gly	NA	NA	+	-	MR, TR
NS185	4	c.170C>G	p.Ala57Gly	NA	NA	+	+	ASD, PDA
NS216	4	c.170C>G	p.Ala57Gly	NA	NA	+	-	-
NS402	4	c.170C>G	p.Ala57Gly	WT	WT	+	+	-
NS168	5	c.242A>G	p.Glu81Gly	NA	NA	-	+	VSD
NS410	5	c.244T>G	p.Phe82Val	WT	WT	+	-	-
NS358	5	c.246T>G	p.Phe82Leu	WT	WT	-	+	ASD
NS465	5	c.246T>G	p.Phe82Leu	NA	NA	-	+	VSD
NS276	5	c.247A>C	p.Thr83Pro	WT	WT	+	+	PVC
KCC8	5	c.265T>C	p.Tyr89His	NA	NA	+	+	-
KCC38	5	c.270G>T	p.Met90Ile	WT	WT	+	+	ASD, VSD, PDA
NS234	5	c.284G>C	p.Gly95Ala	WT	WT	-	-	ASD
NS265	5	c.284G>C	p.Gly95Ala	WT	WT	+	+	-
Og22	5	c.284G>C	p.Gly95Ala	NA	NA	-	-	-
Og45	5	c.284G>C	p.Gly95Ala	NA	NA	+	+	ASD

PCR primers used for sequencing are shown in Table S3. Nucleotide changes are not located in CpG dinucleotides, suggesting that they exhibit baseline mutation rates with a phenotypic filtering effect and that only these mutations lead to this phenotype. Abbreviations are as follows: WT, wild-type; HCM, hypertrophic cardiomyopathy; PS, pulmonic stenosis; MVP, mitral valve prolapse; MR, mitral regurgitation; TR, tricuspid regurgitation; ASD, atrial septal defect; PDA, patent ductus arteriosus; VSD, ventricular septal defect; PVC, premature ventricular contraction; and NA, not available.

^aRefSeq NM_006912.5.

^bRefSeq NP_008843.1.

^cHCM and heart anomalies were diagnosed by echocardiography.

single-base substitution (p.Ser35Thr, p.Ala57Gly, p.Glu81Gly, p.Phe82Leu, or p.Gly95Ala) identified in individuals with Noonan syndrome into a pCAGGS expression vector³⁶ harboring *RIT1* cDNA. As an experimental control, cDNAs harboring *RIT1* c.89G>T (p.Gly30Val), c.104G>C (p.Ser35Asn), and c.236A>T (p.Gln79Leu) and *Braf* c.1910T>A (p.Val637Glu) (RefSeq NM_139294), which corresponds to oncogenic p.Val600Glu in humans, were also generated. *RIT1* p.Gly30Val and p.Gln79Leu correspond to oncogenic RAS alterations p.Gly12Val and p.Gln61Leu, respectively. We introduced pFR-luc, pFA2-Elk1, phRLnull-luc, and wild-type (WT) or mutant expression constructs of *RIT1* into NIH 3T3 cells to examine the transcriptional activation by ELK1,^{18,33} a transcription factor that is activated by MAPK. The results revealed that compared with the WT cDNA, all *RIT1* mutations exhibited significant activation. *RIT1* p.Gln79Leu, followed by p.Gly95Ala, p.Ala57Gly, p.Phe82Leu, and p.Glu81Gly, showed the highest ELK1 transactivation, as also shown in a past study³⁷ (Figure 2A). The c.104G>C (p.Ser35Thr) substitution was identified in two affected individuals. *RIT1* p.Ser35Asn, which corresponds to dominant-negative alteration p.Ser17Asn in RAS, has been used as a dominant-negative substitution in cell experiments.³⁸ To examine the functional consequence of p.Ser35Thr, identi-

fied in affected individuals, we compared the ELK1 transactivation in cells expressing p.Ser35Thr and those expressing p.Ser35Asn. Enhanced ELK1 transactivation was observed in cells expressing p.Ser35Thr, but not in cells expressing p.Ser35Asn (Figure 2B). These results suggest that *RIT1* mutations identified in affected individuals were gain-of-function mutations.

RIT1 is expressed ubiquitously in embryonic and adult tissues.^{33,34} *Rit1*-null mice have been shown to grow to adulthood without any apparent abnormalities;³⁹ hence, physiological roles of *RIT1* in development remain unknown. To examine the developmental effect of identified mutations, we introduced mRNA of the WT and three *RIT1* mutations (c.236A>T [p.Gln79Leu], c.242A>G [p.Glu81Gly], and c.284G>C [p.Gly95Ala]) into 1-cell-stage zebrafish embryos and observed the phenotype at 11 hr postfertilization (hpf). An oval-shaped egg sack, a typical manifestation of the gastrulation defect, was observed in embryos expressing *RIT1* alterations (Figure 3A). This characteristic shape change was also observed in zebrafish expressing gain-of-function mutations of human *NRAS*⁴⁰. Next, we observed the phenotype at later stages (48–52 hpf) (Figure 3B and Figure S4). The introduction of the WT mRNA did not interfere with the normal development, resulting in generally normal morphology